ARMA 18-230

Modeling constant height parallel hydraulic fractures with the Elliptic Displacement Discontinuity Method (EDDM)

Protasov, I.I.
Department of Civil Engineering, University of Houston, Houston, TX, USA
Peirce, A.P.
Department of Mathematics, University of British Columbia, Vancouver, BC V6T 1Z2, Canada
Dontsov, E.V.
Department of Civil Engineering, University of Houston, Houston, TX, USA

ABSTRACT: This paper presents a numerical model for the simultaneous growth of multiple parallel hydraulic fractures with a constant height. The model uses an idealized formulation based on the Elliptic Displacement Discontinuity Method (EDDM). The EDDM assumes each fracture element to have displacement discontinuities of an elliptical shape and solves the one-dimensional elasticity problem. In addition to the EDDM, the model employs the multi-scale tip asymptotic solution that allows a coarser mesh near the fracture tip, compared to the LEFM solution. To show the capabilities of the developed model, the paper presents the comparison between the computed numerical solution and a reference solution. The latter is calculated using a fully 3D hydraulic fracturing simulator for multiple parallel hydraulic fractures. We investigate the effect of perforation friction and spacing on the results. The comparison shows that the EDDM model agrees with the reference solution when spacing between fractures is greater than the fracture height. However, a discrepancy appears in the zero perforation friction case once the fracture spacing becomes comparable or smaller than the fracture height.

1. INTRODUCTION

Hydraulic fracturing is a method used to crack rock formations using high-pressure fluid. The technology is often applied in oil and gas well stimulation (Economides and Nolte, 2000), waste disposal (Abou-Sayed et al., 1989), rock mining (Jeffrey and Mills, 2000), and geothermal energy extraction (Brown, 2000). Typically, multiple fractures are simultaneously induced to reduce the operational costs. Therefore, the ability to simulate multiple interacting hydraulic fractures can improve the design of hydraulic fracture treatment. Hydraulic fracturing simulators often use various approximations that affect the accuracy and the computational time of the numerical procedures (Adachi et al., 2007, Olson, 2008, Kresse et al., 2013, McClure and Zoback, 2013, Wu et al., 2015, Peirce and Bunger, 2014, Peirce, 2015, Dontsov and Peirce, 2015a). Constant height hydraulic fractures, considered in this paper, resemble classical Perkins-Kern-Nordgren (PKN) fracture geometry (Perkins and Kern, 1961, Nordgren, 1972). The classical PKN model uses a local elasticity assumption and ignores an essential part of constructing a simulator for multiple growing fractures - the interactions between the fracture elements. This issue is addressed by the enhanced PKN (EPKN) method for a single fracture (Dontsov and Peirce, 2016, Protasov and Donstov, 2017), in which the elastic interactions between cross-sectional elements are based on the elasticity equation for a planar fracture (Adachi and Peirce, 2008). The elliptic fracture opening profile from the classical PKN model is taken as an assumption for the EPKN method making it possible to reduce the planar elasticity equation to a one-dimensional relation. In addition, the EPKN method employs the multiscale tip asymptotic solution (Garagash et al., 2011, Dontsov and Peirce, 2015b) to make it possible to use a relatively coarse mesh near the fracture tip without losing accuracy, compared to the LEFM. As shown in (Dontsov and Peirce, 2016, Protasov and Donstov, 2017), the EPKN method possesses a high computational efficiency, compared to the fully planar simulators, while being able to accurately predict fracture size for a wide set of parameters.

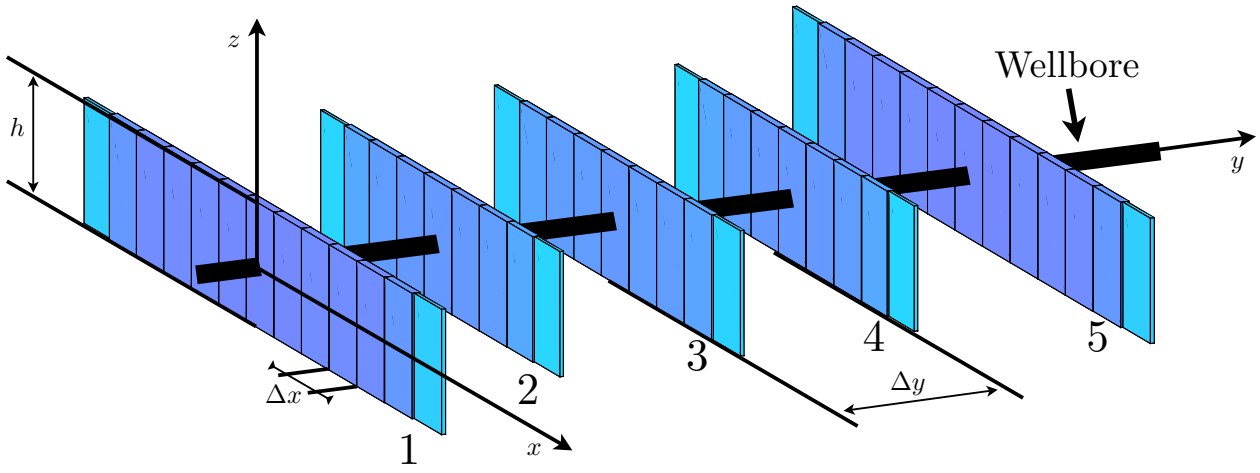

Fig. 1. A schematic of the hydraulic fracture geometry with coordinate system x, y, z. The fluid, injected into the wellbore, drives the horizontal propagation of five equally spaced parallel hydraulic fractures along the x-axis. The fractures with height h are restricted from vertical growth by confinement layers. The spacing Δy between fractures is uniform. The numerical procedure discretizes the fractures into elements with length Δx along x direction. Fractures are numbered from 1 to 5, but due to symmetry, the fractures 1 and 2 are identical to the fractures 5 and 4.

This study is dedicated to the extension of the EPKN model (Protasov and Donstov, 2017) to the case of multiple parallel constant-height hydraulic fractures. This is done by extending the elasticity calculation procedure from the EPKN model to the elliptic displacement discontinuity method (EDDM). The classical displacement discontinuity method (DDM) (Crouch and Starfield, 1983) provides an analytical solution for the fracture-induced stresses in form of a two-dimensional integral over the fracture surface. The common procedure in the DDM is to discretize fractures into piece-wise constant elements for the purpose of numerical integration and collocation at element centers. In contrast to the two-dimensional discretization used in the classical DDM approach, the EDDM employs one-dimensional mesh, since the EPKN elliptic fracture opening assumption allows us to analytically reduce two-dimensional numerical integration. A similar method for simulating multiple interacting hydraulic fractures is presented in (Wu and Olson, 2015), where each fracture element is assumed to have a constant opening in the height direction also allowing for the analytical calculation of the DDM integrals. Since the fracture opening is constant, additional correction coefficients are introduced to account for the fracture width variation in the vertical direction. One of the advantaged of the EDDM is that it does not rely on any correction factors because it automatically accounts for the fracture width variation along the height. In addition, similar to the EPKN model (Protasov and Donstov, 2017) the algorithm uses the multiscale tip asymptotic solution to model dynamics of fracture growth.

In this paper, we compare the results of the developed EDDM-based hydraulic fracturing simulator with a reference solution. The latter is obtained using a fully coupled hydraulic fracturing simulator for multiple parallel hydraulic fractures. In particular, we investigate the influence of the fracture spacing and height on the accuracy of the solution. To achieve this goal, a test problem comprising simultaneously propagating five parallel constant height hydraulic fractures is considered.

2. MATHEMATICAL MODEL

2.1. Problem Formulation

We consider five planar hydraulic fractures propagating perpendicularly to the wellbore, which are restricted from vertical height growth as shown in the hydraulic fracture scheme illustrated in Fig. 1. Within the given x, y, z coordinate system, the wellbore is located along the y axis, each fracture is contained in the (x, z) plane and can be translates in the y direction, uniform fracture spacing Δy is used, and h denotes the fracture height. The simulator can handle a different number of fractures and the spacing between them can also be changed. The rock is modeled as a homogeneous linear elastic material characterized by a Young's modulus E, Poisson's ratio ν, and mode I fracture toughness K_{Ic}. The fluid flow is laminar and the fluid is considered to be an incompressible Newtonian fluid with dynamic viscosity μ. Leak-off is included in the simulator via Carter's leak-off model [5] with a leak-off coefficient C_L, which represents a one-dimensional leak-off perpendicular to the fracture surface. We assume the fluid lag to be negligible. The total volumetric fluid injection rate Q_0 is distributed between fractures depending on the perforation friction.

2.2. Elliptic Displacement Discontinuity Method

We utilize the Elliptic Displacement Discontinuity Method (EDDM), which is an extension of the method used in the EPKN model (Dontsov and Peirce, 2016) to represent the elastic interaction between multiple fractures. The method involves dividing the fracture into multiple elements along its length (x-direction) as shown in the hydraulic fracturing scheme in Fig. 1. The displacement discontinuity is a jump of a displacement vector across fracture surface. In the EDDM method we focus on the displacement components u_x, u_y, which are assumed to have an elliptic profile in a vertical cross-section, as shown in the unit fracture element scheme in Fig. 2, where a fracture element has length Δx, height h, and opening w. In this case

$$\begin{aligned} u_x(x,+0,z) - u_x(x,-0,z) &= \frac{4}{\pi} D_s(x) \sqrt{1-\left(\frac{2z}{h}\right)^2}, \\ u_y(x,+0,z) - u_y(x,-0,z) &= \frac{4}{\pi} D_n(x) \sqrt{1-\left(\frac{2z}{h}\right)^2}, \end{aligned} \tag{1}$$

where normal D_n and shear D_s displacement discontinuities represent the average of the corresponding displacement jumps along fracture height (z-direction). The values D_s, D_n change along fracture length (x-direction) and D_n is the average fracture opening. Each fracture is discretized using piece-wise constant normal and shear displacement discontinuities $D_{n,s}^{(i)}$ along the x direction, so that i_{th} fracture element is defined as

$$D_{n,s}^{(i)} = D_{n,s}\left(x_i\right), \tag{2}$$

where x_i is the coordinate center of the i_{th} element. Let $\mathbf{D_n}$ and $\mathbf{D_s}$ be the normal and shear displacements discontinuity vectors containing the discontinuity components of all the fracture elements:

$$\begin{aligned} \boldsymbol{D_n} &= \{D_n^{(1)}, D_n^{(2)}, ..., D_n^{(N)}\}, \\ \boldsymbol{D_s} &= \{D_s^{(1)}, D_s^{(2)}, ..., D_s^{(N)}\}. \end{aligned} \tag{3}$$

Similarly, the stresses are defined at each element center $\sigma_{n,s}^{(i)} = \sigma_{n,s}\left(x_i\right)$ and can be written in a vector form as

$$\begin{aligned} \boldsymbol{\sigma}_n &= \{\sigma_n^{(1)}, \sigma_n^{(2)}, ..., \sigma_n^{(N)}\}, \\ \boldsymbol{\sigma}_s &= \{\sigma_s^{(1)}, \sigma_s^{(2)}, ..., \sigma_s^{(N)}\}, \end{aligned} \tag{4}$$

where $\boldsymbol{\sigma}_n$ is the vector of normal stresses and $\boldsymbol{\sigma}_s$ is the vector of shear stresses.

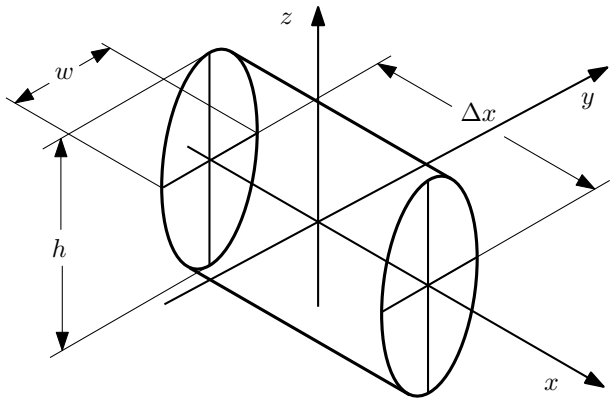

Fig. 2. A unit fracture element used in the numerical procedure with length Δx, height h, and opening w. The element has an elliptic shape due to the assumption of an elliptic displacement discontinuity field.

We refer to a fracture element with elliptic displacement discontinuity variation as an elliptic displacement discontinuity element. According to the Displacement Discontinuity Method (DDM), stress components have a linear relationship to the normal and shear discontinuities and far field stresses as:

$$\begin{aligned} \boldsymbol{\sigma}_n &= \boldsymbol{C}_{nn}\boldsymbol{D}_n + \boldsymbol{C}_{ns}\boldsymbol{D}_s + \boldsymbol{\sigma}_n^*, \\ \boldsymbol{\sigma}_s &= \boldsymbol{C}_{sn}\boldsymbol{D}_n + \boldsymbol{C}_{ss}\boldsymbol{D}_s + \boldsymbol{\sigma}_s^*, \end{aligned} \tag{5}$$

where $\boldsymbol{C}_{nn}, \boldsymbol{C}_{ns}, \boldsymbol{C}_{sn}, \boldsymbol{C}_{ss}$ are the elasticity matrices and $\boldsymbol{\sigma}_n^*, \boldsymbol{\sigma}_s^*$ are the vectors representing the values of the far field stresses in each element. Crouch and Starfield, 1983 solved the elasticity problem of a constant displacement jump over an arbitrarily oriented, rectangular element in an infinite elastic medium by employing the Green's function approach. We utilize this approach to solve the elasticity problem of an elliptic displacement discontinuity element, so that the elements of the elasticity matrices from Eq. (5) can be calculated using the Salamon representation (Crouch and Starfield, 1983):

$$\begin{aligned} C_{nn}^{(i,j)} &= -\frac{E}{8\pi(1-\nu^2)}\left(I_{,yy} - yI_{,yyy}\right), \\ C_{ns}^{(i,j)} &= \frac{E}{8\pi(1-\nu^2)} yI_{,xyy}, \\ C_{sn}^{(i,j)} &= \frac{E}{8\pi(1-\nu^2)} yI_{,xyy}, \\ C_{ss}^{(i,j)} &= -\frac{E}{8\pi(1-\nu^2)}\left(I_{,yy} + \nu I_{,zz} - yI_{,xxy}\right), \end{aligned} \tag{6}$$

where $I_{,ij}$ are the derivatives of the integral of the Newto-

nian potential:

$$
\begin{aligned}
&I(x,y,z) = \\
&= \int\limits_{-\frac{\Delta x}{2}}^{\frac{\Delta x}{2}} \int\limits_{-\frac{h}{2}}^{\frac{h}{2}} \frac{4}{\pi} \frac{\sqrt{(1-(2z'/h)^2)}}{\sqrt{(x-x')^2+(z-z')^2+y^2}} dx'dz' \\
&= \int\limits_{-\frac{\Delta x}{2}}^{\frac{\Delta x}{2}} \hat{I}(x,x',y,z)dx'.
\end{aligned}
\tag{7}
$$

Here the integral is evaluated at $x = x_i - x_j,\ y = y_i - y_j,\ z = 0$, where i and j correspond to the particular location in the elasticity matrix. The function $\hat{I}(x,x',y,z)$ in Eq. (7) can be computed analytically.

2.3. Boundary conditions on the fluid-solid interface

The traction on the boundary between solid and fluid has to be continuous and, thus, the normal stress on a fracture surface has to be equal to the negative fluid pressure, and the shear stress has to be zero in order to satisfy the no-slip condition for fluid contacting solid:

$$
\begin{aligned}
&\boldsymbol{\sigma}_n = -\boldsymbol{p}, \\
&\boldsymbol{\sigma}_s = 0.
\end{aligned}
\tag{8}
$$

Here $\boldsymbol{p}$ is a vector containing fluid pressure in all fracture elements.

Combining these boundary conditions with Eq. (5) yields

$$
\boldsymbol{p} = \mathbb{C}\boldsymbol{D}_n - \boldsymbol{\sigma}^*, \tag{9}
$$

where the full elasticity matrix $\mathbb{C}$ and the full far field stress $\boldsymbol{\sigma}^*$ are defined in terms of the Schur Complement as follows:

$$
\begin{aligned}
&\mathbb{C} = -(\boldsymbol{C}_{nn} - \boldsymbol{C}_{ns}\boldsymbol{C}_{ss}^{-1}\boldsymbol{C}_{sn}), \\
&\boldsymbol{\sigma}^* = (\boldsymbol{\sigma}_n^* - \boldsymbol{C}_{ns}\boldsymbol{C}_{ss}^{-1}\boldsymbol{\sigma}_s^*).
\end{aligned}
\tag{10}
$$

This expression provides a relation between fluid pressure and fracture opening, which incorporates shear stress free boundary condition at the fracture surface.

2.4. Lubrication equation

Since we consider the fractures propagating horizontally along their length (x-direction) and restricted from vertical growth (z-direction), the fluid balance in each fracture has the following form:

$$
\frac{\partial w_k}{\partial t} + \frac{\partial q_k}{\partial x} + \frac{2C_L}{\sqrt{t - t_{0,k}(x)}} = \frac{Q_k}{h}\delta(x), \tag{11}
$$

where the last term on the left hand side captures the fluid leak-off according to Carter's model; w_k is the average opening of the k-th fracture, which, once discretized, is equal to the normal displacement discontinuity D_n of that fracture; $t_{0,k}(x)$ is the time instant at which the k-th fracture tip was located at the point x; Q_k is the fluid flux that enters k-th fracture; and q_k is a fluid flow rate, which can be calculated based on Poiseuille flow of a Newtonian fluid in an elliptic DDM element of k-th fracture as:

$$
q_k = -\frac{w_k^3}{\pi^2\mu}\frac{\partial p_k}{\partial x}. \tag{12}
$$

Eq. (11) applies for all displacement discontinuity elements. The distribution of fluxes entering each fracture depends on the perforation friction, but the total flux Q_0 in the wellbore is prescribed.

$$
\begin{aligned}
&\sum Q_k = Q_0, \\
&p_k + p_{pf,k} = p_0,
\end{aligned}
\tag{13}
$$

where p_k is the pressure at the injection point of the k-th fracture, $p_{pf,k}$ is the pressure loss on friction at k-th perforation, and p_0 is the pressure in wellbore.

2.5. Boundary conditions at the moving fracture tip

The linear elastic fracture mechanics solution is often valid only in a small region near the fracture tip (Garagash et al., 2011), which imposes a restriction to use a very fine mesh. In order to avoid this limitation, we incorporate the approximate multiscale asymptotic solution (Dontsov and Peirce, 2015b, Dontsov, 2017), as a boundary condition to account for the effect of fluid viscosity and leak-off near the fracture tip region at a larger scale. In this case, the boundary condition near the fracture tip can be written as

$$
w(s) \approx w_a(s), \quad s = o\left(L\right), \tag{14}
$$

where s is the distance from the tip, $w_a(s)$ is the fracture opening from the multiscale asymptotic solution, and L is the characteristic length of the fracture. The multiscale asymptotic solution w_a can be calculated by considering the problem of a semi-infinite hydraulic fracture propagating steadily with the velocity V under plane strain conditions (Garagash et al., 2011, Peirce and Detournay, 2008).

2.6. Reference solution

The Implicit Level Set Algorithm (ILSA) (Peirce and Detournay, 2008, Peirce and Bunger, 2014, Dontsov and Peirce, 2017) is a displacement discontinuity-based hydraulic fracturing simulator capable of modeling multiple planar hydraulic fractures in elastically isotropic elastic media. ILSA gradually changes the position of the fracture front within each tip element to capture the necessary multiscale behavior associated with the tip asymptotic solution. For our study, we use ILSA solutions to evaluate the accuracy of the developed EDDM method.

(a) Five hydraulic fractures with 20 m spacing, EDDM results.

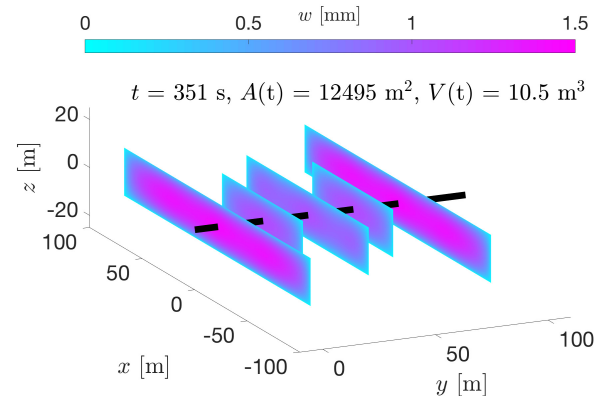

(b) Five hydraulic fractures with 20 m spacing, ILSA results.

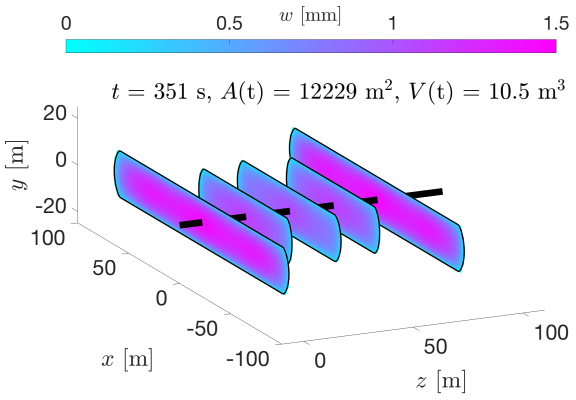

(c) Fracture surface area vs time, spacing 20 m.

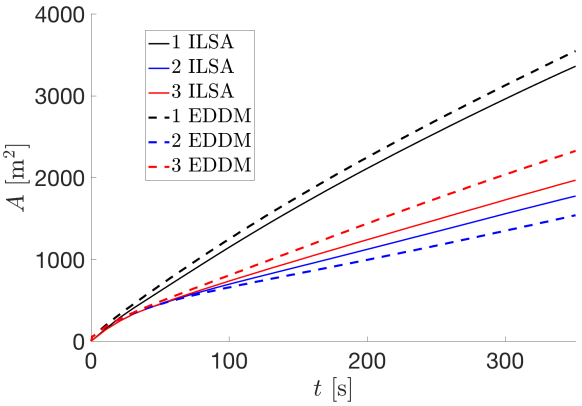

(d) Fracture surface area vs spacing, time $t = 351$.

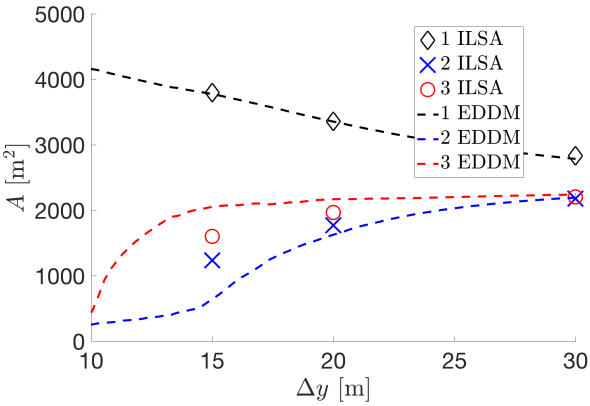

Fig. 3. A comparison of the EDDM and reference (ILSA) numerical solutions for the simulation of five parallel constant height hydraulic fractures. This **no perforation friction case** exhibits significant stress shadowing. (a) and (b) show fracture footprints for spacing $\Delta y = 20$ m at time $t = 351$ s computed by the EDDM and ILSA respectively. (c) shows the comparison of the fracture surface area vs time for the two models with spacing $\Delta y = 20$ m. The numbers in the legend denote fracture numbers considering the symmetry of the problem, see Fig. 1. (d) shows the difference in computed fracture surface area for different values of spacing at time $t = 351$ s.

3. RESULTS

In this section we present the numerical solution computed using the developed EDDM model and compare it to the reference solution (ILSA). The comparison is made for the problem of five equally spaced parallel hydraulic fractures restricted from vertical growth.

The material parameters in the simulation are the following: Young's modulus $E = 20$ GPa, Poisson's ratio $\nu = 0.2$, fracture toughness $K_{Ic} = 1.6$ MPa$\sqrt{\text{m}}$, fluid viscosity $\mu = 3 \cdot 10^{-3}$ Pa·s. In this simulation we consider no fluid leak-off but the EDDM model is able to capture non-zero leak-off. Constant wellbore injection rate of $Q_0 = 0.03$ m^3/s is used and the flux distribution between fractures depends on the perforation friction. We present a series of simulations for different test cases without perforation friction and with large perforation friction. In addition, spacing Δy between fractures varied from 5 to 30 m. The fracture height is taken as 20 m in all cases.

The results of the simulations for the case of no perforation friction are presented in Fig. 3. Fig. 3a shows the final fracture geometry that is computed using the EDDM model at time instant $t = 351$ s and for the spacing $\Delta y = 20$ m. The numerical solution can be visually compared to the same result that is obtained using the reference ILSA solution in Fig. 3b. As can be seen from the figure, there is a reasonable agreement between the two approaches.

The black line around the fracture footprint in Fig. 3b denotes the exact position of the fracture front in ILSA. Since ILSA is a 3D hydraulic fracturing simulator, the front of each fracture is curved. The standard fracture front in the EDDM is flat. It is possible to include a curved fracture front to further increase the accuracy of the model at early times, when fracture is closer to a radial crack [10].

The evolution of fracture surface area versus time is provided in Fig. 3c. The solutions of the EDDM and ILSA are superimposed for comparison for spacing $\Delta y = 20$ m.

(a) Five hydraulic fractures with $\Delta y = 20$, EDDM results.

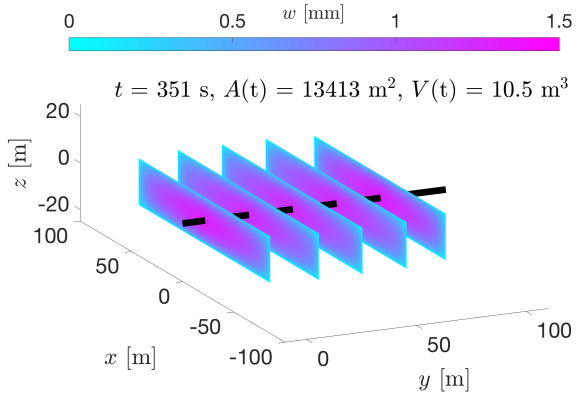

(b) Five hydraulic fractures with $\Delta y = 20$, ILSA results.

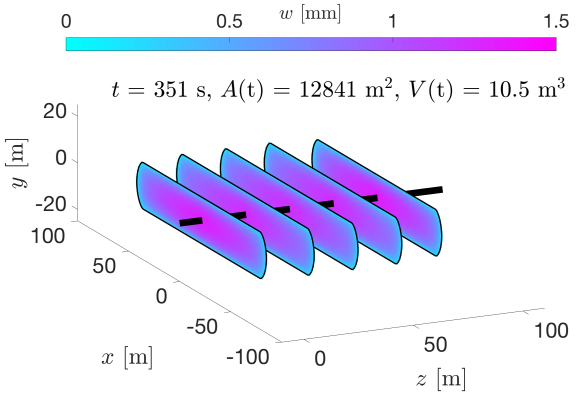

(c) Fracture surface area vs time, $\Delta y = 20$ m.

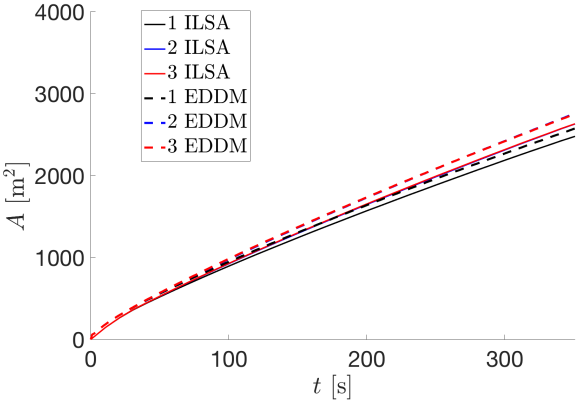

(d) Fracture surface area vs spacing Δy, time $t = 351$.

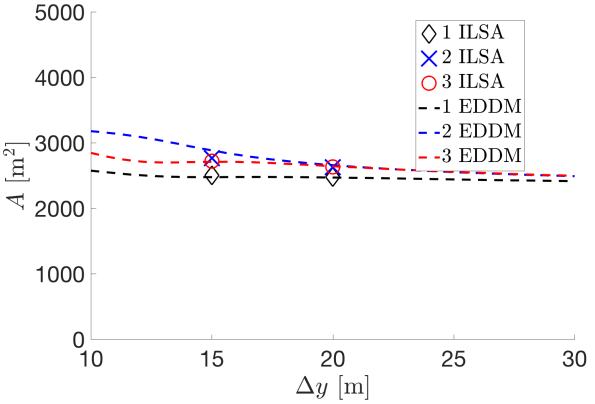

Fig. 4. A comparison of the EDDM and reference (ILSA) numerical solutions for the simulation of five parallel constant height hydraulic fractures. This **even flux distribution case** exhibits very little stress shadowing. (a) and (b) show fracture footprints for spacing $\Delta y = 20$ m at time $t = 351$ s computed by the EDDM and ILSA respectively. (c) shows the comparison of the fracture surface area vs time for the two models with spacing $\Delta y = 20$ m. The numbers in the legend denote the fracture numbers considering the symmetry of the problem, see Fig. 1. (d) shows the difference in computed fracture surface area for different values of spacing Δy at time $t = 351$ s.

The numbers in the legend denote fracture numbers as in the hydraulic fracturing problem scheme defined in Fig. 1. Due to symmetry, fractures 5, 4 have the same properties as fractures 1, 2, thus they are not present in the figure.

The dependence of the fracture surface area on spacing Δy between the fractures is given in Fig. 3d. Here, the results are compared at time instant $t = 351$ s. The ILSA results are shown by markers due to scarcity of the computed results, while EDDM results are plotted by lines. This is dictated by computational efficiency of the algorithms. Each ILSA result for time $t = 351$ s takes approximately 40 hours to compute. At the same time, EDDM is able to provide a result for similar problem within 10 minutes.

The discrepancy between the results in Fig. 3d for $\Delta y < 20$ m can be explained by the difference in real fracture shape versus the elliptic shape used as an assumption in the EDDM model. Lower values of spacing between fractures lead to increased pressure on the central part of the inner fractures. This increased pressure can change the real fracture shape. The elliptic fracture shape assumption may influence the pressure values that are used in the calculation of the flux distribution. The assumption becomes inaccurate when spacing is equal or lower than the fracture height. However, the computationally efficient EDDM model captures the approximate behavior of the fracture propagation for the case of zero perforation friction.

The results of simulations for the case of large perforation friction (which leads to a uniform flux distribution) are presented in Fig. 4. Fig. 4a and 4b show the fracture footprints for spacing $\Delta y = 20$ m computed with the EDDM and ILSA, respectively. The evolution of fracture surface area versus time for spacing $\Delta y = 20$ m is shown in Fig. 4c, where the EDDM and ILSA solutions are put together for comparison. The variation of fracture area versus spacing Δy is given in Fig. 4d for time instant $t = 351$ s. Large perforation friction results in an almost uniform flux distribution among the fractures and therefore all fractures have approximately the same volume. However, since inner fractures are pressurized by outer

fractures, they are longer and have larger surface area compared to the outer ones as can be seen from Fig. 4a and 4b. The EDDM model shows a good agreement with the reference solution for the case of large perforation friction as can be seen from the evolution of the fracture surface area versus time in Fig. 4c. Variation of the fracture surface area versus spacing Δy, shown in Fig. 4d, indicates that the EDDM agrees with the reference ILSA solution for the various spacings considered. The fact that the EDDM model gives more accurate results for large perforation friction than zero perforation friction shows that elliptic fracture shape assumption may influence the flux distribution calculation.

4. SUMMARY

This paper presents a developed EDDM hydraulic fracturing simulator for modeling simultaneous growth of multiple parallel constant height hydraulic fractures. This simulator is the extension of the original EPKN simulator for a single fracture. One of the basic assumptions is that fracture has normal and shear displacement discontinuities of elliptical shape, which allows us to reduce the elasticity problem from a two-dimensional to a one-dimensional, which leads to the elliptic displacement discontinuity method. The other feature of the algorithm is the multiscale tip asymptotic solution that can accurately capture effects of fluid viscosity and fracture toughness, which increases computational efficiency of the developed simulator by allowing a coarser mesh. The EDDM simulator uses a fixed mesh algorithm, which can allow for a further extension to model curved fractures. In order to verify the developed model, we compare it to the fully 3D hydraulic fracturing simulator for multiple parallel hydraulic fractures. In particular, we consider five uniformly spaced parallel constant height fractures. We investigate the effect of perforation friction and spacing on the results. The EDDM model agrees with the reference solution when spacing between fractures is greater than the fracture height. A discrepancy in the flux distribution appears for the zero perforation friction case when the fracture spacing becomes comparable or smaller than the fracture height. However, the EDDM model can handle the considered problem within several minutes on a regular computer.

ACKNOWLEDGEMENTS

Start up funds provided by the University of Houston are greatly acknowledged.

REFERENCES

1. Abou-Sayed, A.S., D.E. Andrews, and I.M. Buhidma. 1989. Evaluation of oily waste injection below the permafrost in Prudhoe Bay field. In *Proceedings of the California Regional Meetings, Bakersfield, CA, Society of Petroleum Engineers*, pages 129-142.

2. Adachi, J., E. Siebrits, A. Peirce, and J. Desroches. 2007. Computer simulation of hydraulic fractures. *Int. J. Rock Mech. Min. Sci.*, 44:739–757.

3. Adachi, J. and A.P. Peirce. Asymptotic Analysis of an Elasticity Equation for a Finger-Like Hydraulic Fracture 2008. *Journal of Elasticity*, 90, 43-69.

4. Brown, D.W. 2000. A hot dry rock geothermal energy concept utilizing supercritical co_2 instead of water. In *Proceedings of Twenty-Fifth Workshop on Geothermal Reservoir Engineering Stanford University, Stanford, California*.

5. Carter, E.D. 1957. Optimum fluid characteristics for fracture extension. In *Drilling and production practices*, 261–270.

6. Crouch, S.L. and A.M. Starfield. 1983. *Boundary element methods in solid mechanics*. London: George Allen and Unwin.

7. Dontsov, E.V. 2017. An approximate solution for a plane strain hydraulic fracture that accounts for fracture toughness, fluid viscosity, and leak-off. *Int. J. Fract.*, 205:221–237.

8. Dontsov, E. and A. Peirce. 2015a. An enhanced pseudo-3D model for hydraulic fracturing accounting for viscous height growth, non-local elasticity, and lateral toughness. *Eng. Frac. Mech.*, 142:116–139.

9. Dontsov, E. and A. Peirce. 2015b. A non-singular integral equation formulation to analyze multiscale behaviour in semi-infinite hydraulic fractures. *J. Fluid. Mech.*, 781: R1.

10. Dontsov, E.V. and A. P. Peirce. 2016. Comparison of toughness propagation criteria for blade-like and pseudo-3d hydraulic fractures. *Eng. Frac. Mech.*, 160:238–247.

11. Dontsov, E.V and A.P. Peirce. 2017. A multiscale Implicit Level Set Algorithm (ILSA) to model hydraulic fracture propagation incorporating combined viscous, toughness, and leak-off asymptotics. *Comp.Meth. in Appl. Mech. and Eng.*, 313, pp. 53-84.

12. Economides, M.J. and K.G. Nolte, editors. 2000. *Reservoir Stimulation*. John Wiley & Sons, Chichester, UK, 3rd edition.

13. Garagash D.I., E. Detournay, and J.I. Adachi. 2011. Multiscale tip asymptotics in hydraulic fracture with leak-off. *J. Fluid Mech.*, 669:260–297.

14. Jeffrey, R.G. and K.W. Mills. 2000. Hydraulic fracturing applied to inducing longwall coal mine goaf falls. In *Pacific Rocks 2000, Balkema, Rotterdam*, pages 423-430.

15. Kresse, O., X. Weng, H. Gu, and R. Wu. 2013. Numerical modeling of hydraulic fracture interaction in complex naturally fractured formations. *Rock Mech. Rock Eng.*, 46: 555–558.

16. McClure, M.W. and M.D. Zoback. 2013. Computational investigation of trends in initial shut-in pressure during multi-stage hydraulic stimulation in the barnett shale. In *Proceedings of the 47nd U.S. Rock Mechanics Symposium. San Francisco, CA, USA*.

17. Nordgren, R.P. 1972. Propagation of vertical hydraulic fractures. In *Soc. Petrol. Eng. J.*, pages 306–314.

18. Olson, J.E. 2008. Multi-fracture propagation modeling: Applications to hydraulic fracturing in shales and tight gas sands. In *Proceedings of the 42nd U.S. Rock Mechanics Symposium. San Francisco, CA, USA*.

19. Peirce, A.P. 2015 Modeling multi-scale processes in hydraulic fracture propagation using the implicit level set algorithm. *Comp. Meth. in Appl. Mech. and Eng., 283:881-908*.

20. Peirce, A.P. and A.P. Bunger. 2014 Interference fracturing: Non-uniform distributions of perforation clusters that promote simultaneous growth of multiple hydraulic fractures. *SPE 172500*.

21. Peirce, A. and E. Detournay. 2008. An implicit level set method for modeling hydraulically driven fractures. *Comput. Methods Appl. Mech. Engrg.*, 197:2858–2885.

22. Perkins, T.K. and L.R. Kern. 1961. Widths of hydraulic fractures. In *J. Pet. Tech. Trans. AIME*, pages 937–949.

23. Protasov, I. and E. Donstov. 2017 A comparison of non-local elasticity models for a blade-like hydraulic fracture In *Proceedings of the 51st U.S. Rock Mechanics/Geomechanics Symposium, San Francisco, CA, USA*

24. Wu, K., J. Olson, M.T. Balhoff, and W. Yu. 2015. Numerical analysis for promoting uniform development of simultaneous multiple fracture propagation in horizontal wells. In *Proceedings of the SPE Annual Technical Conference and Exhibition, SPE-174869-MS*.

25. Wu, K., J. Olson. 2015. A simplified three-dimensional displacement discontinuity method for multiple fracture simulations. *Int. J. Frac. 193(2)*